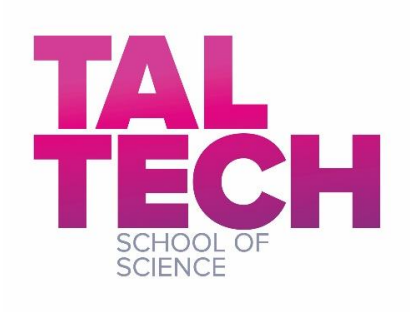

Probing Symmetry Agility by One- and Two-Photon Absorption in Molecular-Star Systems and DNA Analogs

Master thesis

Student: Katarzyna Helena Zneykus
Student code: 230397YAFM
Supervisor: PhD Charles William Stark, researcher
Study program: Applied Physics

Tallinn 2024

Declaration

Hereby I declare that I have compiled the paper independently and all works, important standpoints and data by other authors have been properly referenced and the same paper has not been previously been presented for grading.

Author: [Name]
[Signature, date]

The paper conforms to requirements in force.
Supervisor: [name]
[Signature, date]

Table of Contents

Abstract

Agile materials are those which can alter their functional properties on demand. Such dynamic behaviour typically stems from specific changes to structure on a molecular level, especially in organic systems. One such molecular property with far reaching consequences is symmetry, which can govern the formation of molecular dipoles and drive molecular interactions, as well affect charge-transfer processes and colour changes. Such modulation makes symmetry agile substances well suited for applications of sensing, switching, or storing information. Symmetry switching can also be said to be the driving force behind the reaction centres of many proteins, and biological functional groups like hemes, which use subtle local conformational disturbances to govern reactivity. By comparison, man-made symmetry agile materials are relatively rare, and discussion of "molecular symmetry breaking" is typically done using a series of similar molecular systems, which typically do not interconvert their symmetric structure, or perhaps only break symmetry in the excited state. However, as most molecular processes occur in the ground state, improving investigation capabilities of these processes is crucial to understanding their potential.

Here, one- and two-photon excitation is used to investigate two molecular systems, which display interconversion of molecular structure in the ground state. The first system, is a star-shaped ethynyl-benzene compound with proton-accepting pyridine tips. This compound is observed to undergo three acid-base reactions, which initially break the high-symmetry of the ground state, causing an increase in two-photon absorption, indicative of an enhanced charge-transfer process. Conversely, the neutral state demonstrates a forbidden lowest energy absorption band, which is surprisingly highly-fluorescent compared to the other acidic forms. These features make this molecular system interesting for both sensing and photoredox chemistry.

Additionally, absorption of a DNA base analogue, 2-aminopurine, is investigated using dichroic methods leading to the two-photon polarization ratio, which reveals differences in absorption for the 7H- and 9H- tautomeric forms. These forms are able to be separated spectrally in what may be the first demonstration of this process. Such tautomerization is common place in DNA, making interaction mechanisms very complex, so this is a crucial step towards unravelling such ground-state molecular puzzles.

1. Introduction

1.1. The dark world of ground state dynamics

Molecular structure governs many material properties; a fact that is especially true for organic systems, where subtle changes to molecular structure garner wide ranging effects in chemical and biochemical behaviour. As such, molecular systems which may controllably change chemical structure hold promise for designing agile materials that may tune functionality on command. Such systems would be useful for data storage,[1,2] sensing,[3] molecular machines,[4] and other applications. However, such materials are inherently complicated as a result of multiple stable configurations, for which fundamental investigations of properties such as ground-state symmetry-breaking,[5,6] could be greatly illuminating.

One of the main limitations to understanding molecular behaviour, particularly in regards to ground state electronic behaviour, is that the associated dynamics is often hard to observe. The majority of studies investigating molecular electronic mechanisms are conducted using time-resolved excited state methods, such as transient absorption,[7] time-resolved emission,[8] time resolved resonant Raman,[9] or others.[10,11] Because excited states can be created with an impulse, they may controllably reveal a great many molecular processes as well as the timescales on which those processes occur. Some excited state dynamics involve so called 'dark' states, which are unable to be seen directly using the particular method, but can be inferred from the dynamics of other observed states. However, for molecules in the ground state, comprising the vast majority in any given system, there are no 'relaxation' pathways that can be monitored, so all dynamic behaviour that may exist here can be considered 'dark'.

Absorption spectroscopy, whereby a photon is used to excite a ground-state molecule into an instantaneously formed (vertical) excited state, is perhaps the most well-known optical method for accessing ground state molecular properties. However, many studies investigating symmetry focus on non-switching systems,[12–14] which constrain molecules of a known molecular symmetry, but where these systems do not change form, so the effect of switching cannot be directly measured. Such lists of chemical analogues may also corrupt their investigation process by imparting new features from the modifications themselves rather than strictly as a result of changes in symmetry.

Two photon absorption (2PA) is an extension of absorption processes, which expands capabilities of ground state investigations by having of unique symmetry rules[15] and novel dichroic phenomena.[16] In particular, molecules which can switch their ground state nature, through changes in molecular symmetry or by other means, may be dramatically better understood by comparing 1PA and 2PA response. This understanding, in turn, could enable better design of ground-state switching devices for future technologies.

1.2 Absorption of light: One- and two-photon processes

Absorption of light occurs when one (or several) photons are absorbed by a chromophore and result in an excited state of that chromophore.[17] A chromophore, called so because it induces a colour in a material, may be a molecule, a specific sub-group in that molecule (e.g., in a supermolecular assembly), or even several molecules interacting together (e.g., in an excimer),

which becomes electronically excited. In any case, the primary attribute of a chromophore is that it has an energy, *E*, between the ground and excited state, called the transition energy, which corresponds to a particular wavelength, λ, in the visible (400 – 750 nm), ultraviolet (10 – 400 nm), or near-infrared (750 – 1500 nm) regions of the electromagnetic spectrum,

$$E = \frac{hc}{\lambda}$$

where *h* is the Planck's constant and *c* is the velocity of light. In this form, absorption corresponds to a single photon, with energy equal to the transition energy; however, absorption can also occur from multiple photons together inducing the same transition. To understand the relationship of this absorption, we may use photon flux, Φ, having units of photons/(m^2s) to describe the rate at which photons pass through an area over time,

$$\Phi = \frac{N}{A \cdot t}$$

Where *N* is a number of photons, *A* is an area through which the photons are passing (m^2), and *t* is a time interval (s). Absorption induces a relative decrease in photon flux over a distance, *z*, which can be described using a phenomenological Taylor expansion,

$$\frac{d\Phi_t}{dz} = -\sigma_{1\mathrm{PA}} N_\mathrm{g} \Phi_t - \sigma_{2\mathrm{PA}} N_\mathrm{g} \Phi_t^2 - \sigma_{3\mathrm{PA}} N_\mathrm{g} \Phi_t^3 \ - \cdots$$

which depends on the density of chromophores in the ground state, N_g, and the absorption cross section of each chromophore, sigma. Here, the first term describes one photon absorption (1PA), the second term describes two photon absorption (2PA), and so on. As noted earlier, the higher order processes correspond to transitions to the same energy, so for chromophores with few transition bands, higher order terms can be easily separated by wavelength. Integrating the first term leads to an exponential decay of intensity with respect to chromophore density or pathlength, corresponding to the well understood Beer-Lambert law of absorption.[18]

$$\sigma_t(z) = \sigma_0 e^{-\sigma_{1\mathrm{PA}} N_\mathrm{g} z}$$

Where Φ_0 is the flux prior to any absorption process. In this case, units of cross section (m^2) are often reformatted to easier to comprehend molar absorption (ε, $M^{-1}cm^{-1}$) corresponding to molar concentrations instead of chromophore density.

The second term contains a two-photon cross-section term, 2PA, has units of $(\Phi \cdot N_g \cdot z)^{-1}$ = (m^4·s/photon), which is often measured in Goeppert-Mayer[19] units of 1 GM = 10^{50} cm^4·s/photon. Notably, the "time-frame" involved in this interaction does not correspond to a step-wise process akin to transient absorption, but instead corresponds to the ability to overlap multiple photon wavefunctions to such an extent that an instantaneous transition from all photons together can occur. A demonstration of the instantaneous nature of two photon transitions can be seen from the fact that two-photon excitation was used to determine the duration of attosecond pulses.[20]

Aside from the unique dependence on photon flux dependence, 1PA and 2PA processes differ in their selection rules,[21] offering a key means to analyse symmetry or orientational-based differences in ground state molecular structures. For monochromatic light sources, these different symmetry rules can be summarized that 1PA transitions correspond to excitations in a single axial direction, corresponding to a vector (x,y,z), while 2PA transitions operate as vector-

pairs, producing a tensor of quadratic terms, (xx, yy, zz, xy, xz, yz). Notably, these higher-order functions give rise to new dichroic behaviour in even achiral systems. The most commonly observed of these novel processes is the relative change of circularly and linearly polarized light, termed the polarization ratio, $\Omega_{2PA} = \frac{\sigma_{circ}}{\sigma_{lin}}$.[16]

1.2.1 Molecular dipoles and the origin of absorption cross section

While the molecular cross section corresponds to a constant of absorption per molecule, this has a deeper meaning with respect to the electronic interactions between light and a molecule. Namely, the 1PA molar absorption spectrum can be written as,[22]

$$\varepsilon_{1PA}(\nu) = \frac{N_a}{10^3 \ln 10} \frac{(2\pi)^3 \nu}{3nch} |\mu|^2 \rho(\nu)$$

where, *N*a is Avogadro's constant, *n* is the index of refraction, *c* is the speed of light, *h* is Planck's constant, ν is the frequency of excitation. The function ρ represents the spectral shape of absorption, which is scaled to integrate to 1 over all frequencies, $\int \rho(\nu)\, d\nu = 1$. Finally, μ is the transition dipole of the excitation process, which gives information into the electronic change involved in moving an electron from the ground to excited state.

In the simple case of a single-ground and single-excited state, a similar relationship may be found for two photon cross section (excited with two linear-polarized photons),[22]

$$\sigma_{2PA}(\nu/2) = \frac{(2\pi)^4}{15(nch)^2} |\mu|^2 |\Delta\mu|^2 (2\cos^2\beta + 1) \rho(\nu)$$

Where two new terms appear, $\Delta\mu$ being the change in permanent electric dipole between the ground and excited state, and β being the angle between $\Delta\mu$ and μ. This angle separating the two dipole moments involved gives rise to the polarization ratio between circular and linear polarized light; while circularly polarized light is rather unaffected by angle, linearly polarized light is enhanced for dipole pairs that are also linearly aligned ($\beta \sim 0$).

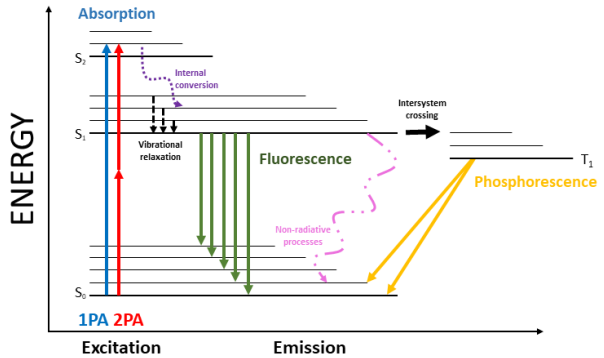

Figure 1. Fluorescence decay pathways. Excitation to S_1 or S_2 excited states may undergo relaxation to the lowest-vibrational S_1 state, which can fluorescence. In some cases, molecules may undergo intersystem crossing to the triplet state, producing analogous phosphorescence.

1.3 Emission

Excited chromophores, due to their excess energy compared to their surroundings, are generally short lived. One mechanism for relaxation back to the ground state is fluorescence, which is essentially an inverted process from absorption,[23] releasing a photon equal to the energy difference between the excited state and the ground state. There are often additional relaxation processes that occur as well, such as vibrational relaxation of a single electronic state, internal conversion between excited electronic singlet states, or intersystem crossing, which transitions between electronic states with differing electronic spin. Often, these nonfluorescent processes are much faster than fluorescence (or phosphorescence in the case of spin-forbidden emission), such that emission of a chromophore always appears from the lowest-energy excited-state, a phenomenon known as Kasha's rule.[24]

This energy loss causes the electron to transition to the lowest vibrational level of S_1. Following the vibrational relaxation, the electron may remain in the excited state for a duration known as the fluorescence lifetime, which is on the order of nanosecond. Eventually, the electron returns to the ground state S_0, emitting a photon in the process. The emitted photon has less energy than the absorbed photon due to the energy lost during vibrational relaxation.[25] This difference in energy between the absorbed and emitted photons is observed as the Stokes shift. The emitted light has a longer wavelength than the absorbed light, which is a characteristic feature of fluorescence.

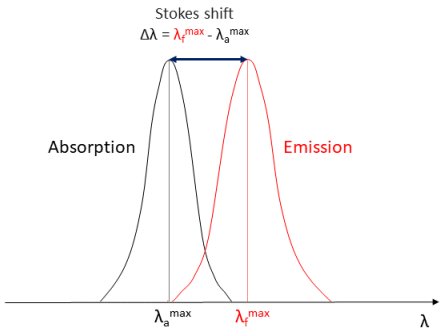

Figure 2. Stokes shift measures the difference between absorption and emission wavelength maxima. It is often used to describe whether a transition has undergone excited state relaxation processes.

The efficiency of the entire emission process is summarized as the quantum yield, which is a ratio of the number of photons emitted to the number of photons absorbed. A high quantum yield indicates that a significant proportion of absorbed photons lead to fluorescence, making the chromophore an efficient emitter.

$$\Phi = \frac{\#\ \text{photons emitted}}{\#\ \text{photons absorbed}}$$

1.4 Dynamic Molecular Symmetry: Symmetry agility and Tautomerism

Molecular symmetry breaking is a phenomenon that is important for many charge-transfer reaction processes. Symmetry breaking is known to prominently participate in excited states dynamics, leading to charge localization and fundamentally driving photocatalysis in many systems.[12] Presumably, ground state symmetry breaking also may occur in many systems, but in this case the process is much harder to observe. One possibility to enforce symmetry breaking processes is to by design of symmetry-agile systems, which have reaction functional groups positioned in symmetric locations, which alter the overall structure of the molecule depending on a reaction parameter.

One of the first forays into this field was performed in 2022,[6] where an inversion symmetric diketopyrrolopyrrole was observed to switch between inversion symmetric and symmetry broken forms, revealing information about the importance of vibrational interactions during initial excitation.

One possible system for controlling symmetry agility using protonation is the compound 1,3,5-tris(pyridine-4-ylethynyl)benzene, hereafter YP3. This structure contains three terminal pyridine groups, which act as proton acceptors, surrounding a benzene core structure. The pyridine ends are linked using acetylene, which have been used as electron-bridges in numerous other charge-transfer systems.[24,26,27,27–30] Using the proton-binding effect of the pyridines, we can probe the molecular symmetry to develop a better understanding of the extent of conjugation and structural stability of the ground state, which is nominally trigonal-planar symmetric (D_{3h}).

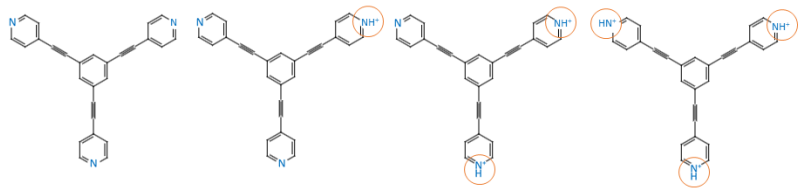

Figure 3. A symmetry-agile molecule reacting at three sites, having trigonal symmetry when all sites are equivalent, while possessing symmetry-broken intermediate reaction states.

Tautomerization is another example of molecular dynamics which are difficult to monitor in the ground state.[31,32] Tautomers are a type of structural isomer, in which bonding configurations are changed, sometimes including the transfer of a proton from one part of a molecule to another. While it is known to occur in many systems, the process is often inferred by observed differences to "hindered" molecular analogues,[33] or using excited state dynamics,[34] which may or may not be representative of the ground state behaviour of the molecule of interest.

One example of a tautomeric structure is 2-Aminopurine, hereafter 2-AP, which is a fluorescent analogue of the DNA base adenine.[35] Its ground state is known to undergo tautomerization between two forms, with a hydrogen atom attached at either the 7H- or 9H- position, shown in Figure 2.

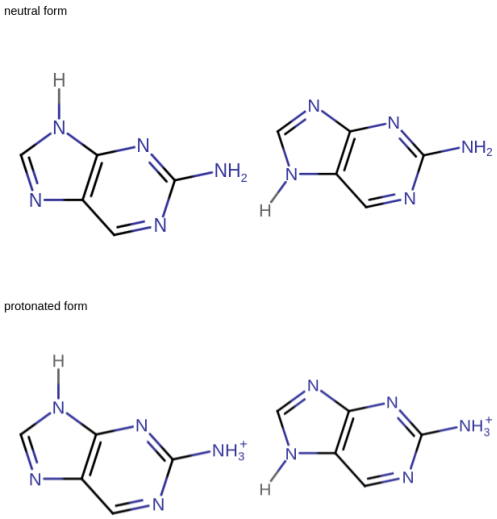

Figure 4. Tautomeric forms 9H- (left) and 7H- (right) for neutral (top) and protonated (bottom) 2-aminopurine structures.

1.5 Protonation & Reaction Equilibria

Protonation is a simple acid-base reaction, wherein a positively charged hydrogen, the proton, is attached to a basic proton-acceptor, forming a bond. This reaction produces a positively charged site on the product molecule, which may have substantial effect on the electronic properties and subsequent spectroscopic features.[6,36] These changes can appear in both 1PA and 2PA, and the two methods may appear differently for the same modification, enabling the interpretation of different states of the molecule. In the cases of symmetry agile systems described here, it acts as a tool used to change the molecular symmetry.

Chemical reactions are always dynamic processes that can transfer molecular reactants into products or vice versa; however, when the formation rate of products from reactants occurs at the same rate as the rate of reactants formed from products, it is said that the chemical process is at equilibrium. For example, an acid dissociation reaction, in which an acid molecule *(HA)* splits into a proton *(H^+)* and the conjugate base molecule *(A^-)*, has a complementary reaction where the charged species recombine written as,

$$HA \rightleftarrows H^+ + A^-$$

At equilibrium, the concentrations of products and reactants are constant, so it can be convenient to write them according to their proportionality, forming a reaction equilibrium equation,

$$K_a = \frac{[H^+][A^-]}{[HA]}$$

Here, K_a represents the acid-dissociation constant, representing the relative propensity for dissociation. In this example, as the dissociation involves breaking bonds and solvating the charged species in some local environment, it will depend on the energies involved in breaking the bond and forming the solvation shell, and in general is dependent on the energetics of the reactants and products involved. However, for chemical equilibria at a given temperature, K_a is indeed a constant.

Importantly, the concentration of H^+ is the solution acidity, which can be affected by additions of acids and bases, as well as monitored using a pH probe ($pH = -\log[H^+]$). This allows for control of the molecular form of HA and A^- by modifying the concentration of H^+. Increasing H^+ forms additional HA, while decreasing H^+ forms A^-. When A^- is equal to HA, then the H^+ concentration is equal to K_a, revealing the value of the acid-base dissociation constant.[37]

2. Experimental methods

2.1 Preparation of the samples

YP3 was obtained from Gryko's group from the University of Warsaw. For experiments a small amount of the powder sample was dissolved in MeOH (HPLC grade, manufactured by Honeywell). For 1PA measurements, samples were prepared at ~5 mM concentration in a 1 cm cuvette, which was also used for fluorescence measurements. For 2PA measurements, samples were ~60 mM contained in a 1 mm cuvette.

2-Aminopurine was purchased from Sigma Aldrich company. For all experiments a small amount of the powder sample was dissolved in water, distilled in-house. Similar to YP3, 1PA samples were analysed in 1 cm cuvette, while 2PA measurements were performed in 1 mm cuvettes.

For acid-base reactions and titration techniques, trifluoromethanesulfonic (triflic) acid (≥99% purity, from Sigma Aldrich) was used, dissolving a stock solution in MeOH or water for use with YP3 or 2AP, respectively. As the strong acid openly reacts to water vapour, molar quantification of the stock solution was not possible, but was inferred from measurements of pH during titration.

Reference 2PA samples of Coumarin 153 (99% purity, Sigma Aldrich) and Prodan (98% purity, Sigma Aldrich) were dissolved in Toluene in 1 mm cuvettes, and characterised to have absorbance of ~0.7 O.D.[38,39]

2.2 One-photon spectroscopy

Figure 5. UV Spectrometer Shimadzu, 3600 PLUS

In all 1PA experiments, an automated spectrometer UV 3600 PLUS, Shimadzu was used in the range 185 – 1200 nm, with 1 nm steps. All measurements were performed by first recording a baseline (I_0) with no cuvette present, and a subsequent spectrum of the cuvette and solvent, before the addition of sample (I_T). In this manner, absorbance ($A = -\mathrm{Log}(I_T/I_0)$) was obtained using

a back-to-back comparison with a single detector. In the case of titration, measured spectral regions were reduced to 185 – 600 nm, so as to save time.

The molar absorption measurement procedure commenced with the precise weighting of 0.0015 g of YP3, which was then deposited into a 25 mL volumetric flask. The flask was filled with MeOH and agitated to ensure thorough mixing. Next, 3 mL of pure MeOH was dispensed into a 1 cm quartz cuvette, and its absorbance was recorded. Successively, 25 µL of the YP3 solution was added to the cuvette and the UV measurement was repeated. This process was iterated until a total of 11 drops, each containing 25 µL of YP3 solution were added with absorbance measurement taken after each addition.

2.2.1 Titration

The solution of YP3 in MeOH was prepared by placing a diminutive amount of YP3 power into a glass vial. Then the vial was filled up with MeOH and shaken until YP3 was visibly dissolved. From this YP3 stock solution, 3 ml was placed in a 1 cm quartz cuvette using a micropipette (PIPETMAN by Gibson) and pH recorded using a Lazar Ultra-M pH electrode connected to a YFE -3505 multimeter with 200 mV sensitivity.

Figure 6. YFE-3505 multimeter and pH electrode (Ag/AgCl).

A dilute solution of triflic acid in methanol was added dropwise (25 - 100 µL) and after each drop the pH was measured and the 1PA spectrum was obtained. These steps were repeated until the solution reached the solvent buffer region near -1 pH.

The solution of 2AP in water was prepared in a similar manner. A small amount of 2AP powder was placed in a glass vial and filled with distilled water, of which 3 ml of solution was placed in 1 cm cuvette and the pH and 1PA measurement were repeated until the full protonation of 2AP.

2.3 Fluorescence spectroscopy

Fluorescence measurements were conducted using a double-grating fluorometer (LS 55,Perkin Elmer). For single emission scans, the excitation wavelength (λ_{ex}) was fixed to a region of maximum 1PA signal, and the emission wavelength (λ_{em}) was scanned from 5 nm above this wavelength, to 10 nm below $2 \cdot \lambda_{ex}$. This emission region was selected to avoid second order diffraction effects.

Two-dimensional scans, which changed both λ_{ex} (280 – 325 nm) and λ_{em} (230 – 550 nm) in a square-grid pattern, were also performed on YP3 samples.

2.4 Two photon absorption

2.4.1 Laser system

The 2PA excited fluorescence measurements were conducted using a femtosecond laser system manufactured by Light Conversion, Ltd. This system included a pump laser (Pharos-SP), optical parametric amplifier (OPA, Orpheus-HE), and second harmonic generator (SHG, Lyra-SH). The pump laser generates femtosecond pulses with duration of 70 - 90 fs and average powers of 0.6 - 2 W. These pulses are amplified in the regenerative amplifier, which uses Yb:KGW as the gain medium. The OPA and SHG components further refine the laser pulses for 2PEF experiments, allowing precise control over wavelength and intensity.

The 1030 nm pump beam is split into three components upon reaching the OPA input, for the application of three main components: white-light continuum generation, pre-amplification (1st amplification stage) and power amplification (2nd amplification stage). The first component is focused on a 1 mm thick sapphire plate, generating a supercontinuum of visible wavelengths. The other two components produce the second harmonic wavelength of the laser at 515 nm using second harmonic generator (SHG) crystals (BBO, Type I). These crystals are oriented to provide phase-matched SHG between vertically polarised 515 nm and horizontally polarised 1030 nm light. The resulting 515 nm photons are combined with the white-light supercontinuum in a 2nd order nonlinear process of difference frequency generation in another BBO crystal, rotated to achieve wavelength-selective phase-matching. This interaction results in the generation of the pre-amplified signal wavelength and an idler wavelength. This down-conversion process conserves energy, ensuring the independence of wavelengths inside the crystal according to

$\nu_{pump} = \nu_{signal} + \nu_{idler}$.

The residual pump and idler beams are blocked, while the pre-amplified seed is directed to the dichroic mirror using mirrors and lenses. This seed beam is then combined with the main amplifying portion of the second harmonic of the pump. Both beams pass collinearly through the 2nd amplifying BBO crystal where the difference signal and idler are further amplified. Both the signal and idler beams exit the crystal nearly colinearly, while the second harmonic of the residual pump is removed by a dichroic mirror. The wavelengths produced in the OPA output range from 630 to 1040 nm for the signal and from 1025 to 2600 nm for the idler, with pulse duration of less

than 170 fs. Additional wavelengths are generated in Lyra-SH via SHG in an additional BBO crystal using either the signal (for 315 – 515 nm) or the idler (for 515 – 630 nm). All BBO crystals, as well as compensating glass plate delay mechanics, are automated using software (WinTopas-4, Light Conversion), which was controlled in our case using a LabVIEW interface.

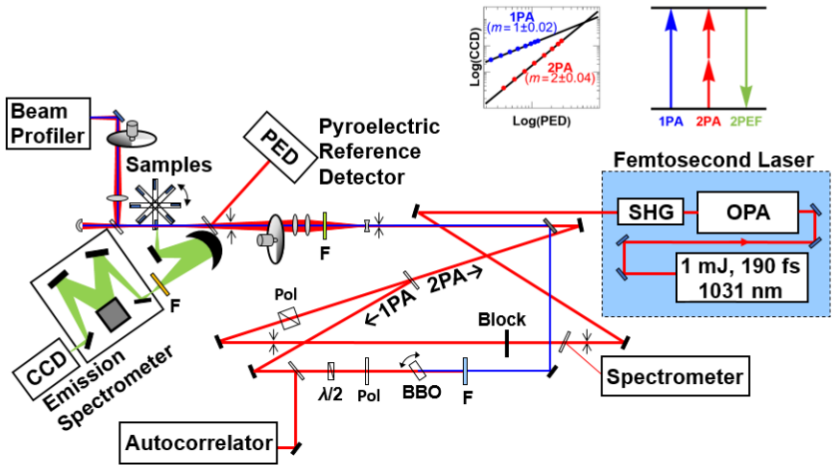

Figure 7. Schematic of 2PA spectrometer. Signals are acquired via two-photon excited fluorescence.

2.4.2 Power dependence

To measure the quadratic power dependence intrinsic to 2PA,[17] laser power was controlled using a neutral density filter wheel (NDC-100C-4, Thorlabs), and monitored using a reference pyroelectric detector (QS-I-Test, Gentec). To ensure that no optical damage occurred on the filter, the beam was expanded 4× using a Galilean telescope consisting of a concave lens (f = -75 mm) followed by a convex lens (f = 300 mm) placed 22.5 cm from one another. A third lens (f = 750 mm) gently focused light ~ 50 mm after the sample, so as to ensure tight nearly-collimated beam character, while not being directly focused to reduce potential higher-order nonlinear processes. This exciting pulse was then directed at a beam dump, while the sample fluorescence was collected at 90 degrees, using a focusing mirror to direct light into a monochromator and charge-coupled device (CCD, Symphony II, Horiba). Power dependence was verified by comparing the two-photon excited fluorescence signal from the CCD to the reference detector while stepping the filter wheel to ~8 discrete positions, controlled via LabVIEW.

Subsequently, data points were analysed by linear fitting a double-log plot using Mathematica. The resulting slope of the log-log fit gave the power dependence, while the lines intercept corresponded to the logarithm of the 2PEF signal, denoted as F.

2.4.3 2PA references and laser correction

Two reference samples were used for all experiments: Coumarin 153 in toluene and Prodan in toluene. These were quantitatively characterized previously in the nonlinear optics lab,[38] and had been improved since publication, with update ed versions found in an online repository.[39]

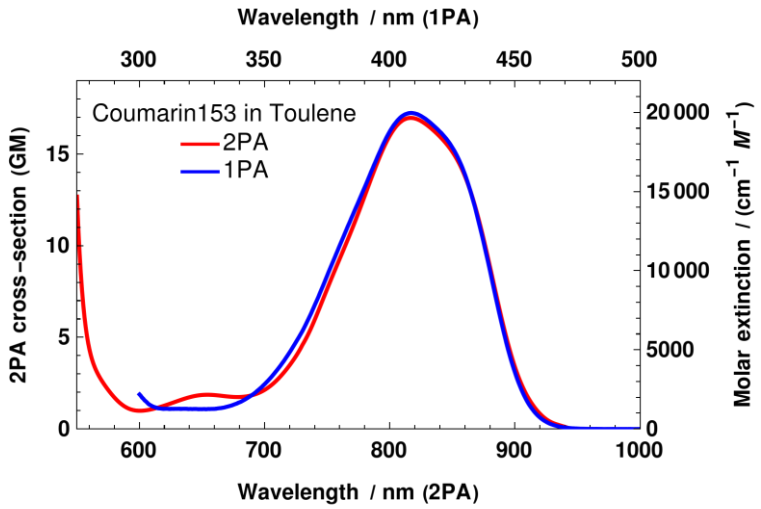

Figure 8. Optical absorption cross sections for Coumarin 153 in toluene. 1PA (Blue line, right axis) and 2PA (Red line, left axis).

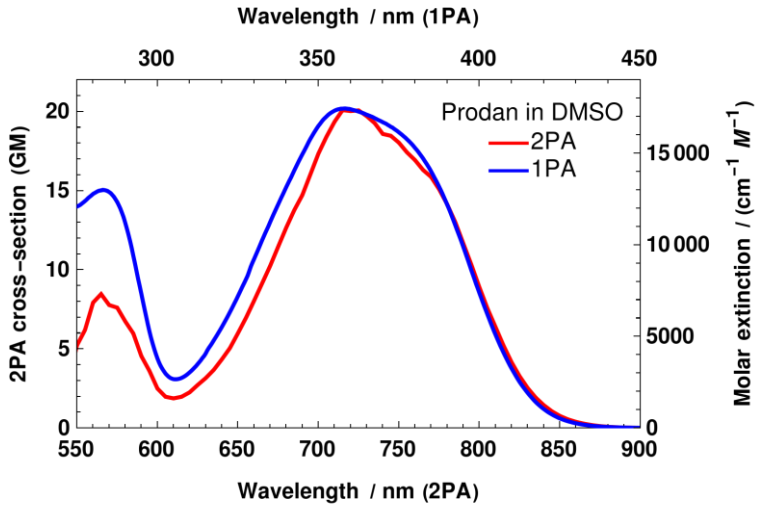

Figure 9. Absorption cross sections for Prodan in toluene. 1PA (Blue line, right axis) and 2PA (Red line, left axis).

These samples, due to their broad spectra covering the range of 550 – 900 nm, and optical stability, were used to correct laser power-density fluctuations for both YP3 and 2AP 2PA measurements. Spectral correction was done by comparing the measured reference 2PA signal to the correct spectrum from the database, multiplying the sample spectrum by this correction factor, $\sigma_s \propto F_s/F_r \cdot \sigma_r$. These corrections were carried using Mathematica.

2.4.4. Polarisation ratio

The measurement of polarisation ratio, $\Omega = F_{circular}/F_{linear}$,[16] in the 2PA spectrometer was automated using two stepper motors fitted to optical rotation stages. One stage placed before the sample rotated a quarter waveplate (AQWP05M-580, Thorlabs) so as to align the fast axis at +45° for right-circular polarization, -45° for left-circular polarization or 0° & 90° for two vertical polarizations. A second stage rotated a polarizer in the fluorescence path, which was oriented at magic angle with respect to the axis of excitation symmetry, shown in Figure 10. Both motors were controlled using LabVIEW software, measuring all four polarization configurations for all samples at each wavelength. The data was analysed in Mathematica software, where an average of right and left circular polarization was used for the ratio, as the nonchiral-nature of compounds resulted in identical signals for both measurements.

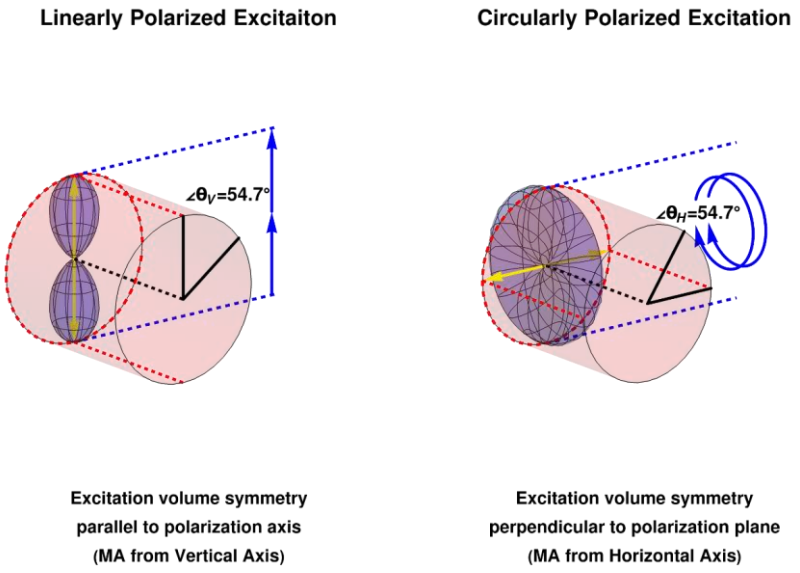

Figure 10. Linearly polarised excitation (left), circularly polarised excitation (right), with emission collected at magic angle polarization from the excitation axis of symmetry.

2.4.5. Absolute absorption

To determine the absolute 2PA cross-section for 2PEF, additional measurements of quantum yield and detector efficiency are necessary. These factors were corrected for by measurement of 1PEF using the same system at wavelengths corresponding to those used in 2PA, i.e., exciting at half the wavelength of 2PEF and collecting the same emission wavelength for both measurements.

To measure 1PEF, a glass plate beam splitter reflects ~ 4% of the excitation beam energy, which then passes through a half-wave plate to alter the polarization from vertical to horizontal. A BBO nonlinear crystal generates a small amount of second harmonic (Type II) realigning the polarisation back to the vertical direction. A short-pass colour glass filter absorbs the residual signal beam. A flip mirror redirects this SHG beam along the same optical path as the 2PA excitation beam, and the beam position on the sample was monitored with a CCD camera to ensure overlap with the 2PEF excitation beam. Due to the vastly weaker signal of the excitation beam, the reference pyroelectric detector was replaced with a photodiode in the same location (Thorlabs), which acted as the reference for fitting the linear power-dependence in the same manner as was done for 2PA measurements.

This measurement of absolute 2PA cross-section assumes that the fluorescence spectrum and efficiency (fluorescence quantum yield and detector efficiency) are constant for both 1PEF and 2PEF in each sample. Measuring 1PEF additionally allows for estimation of differing quantum yield values between the sample and reference, although these were not measured due to the limited overlap of sample and reference emission spectral profiles. The absolute 2PA cross-section of the sample can be calculated using the following formula:[40]

$$\sigma_{2PA}^{S}(\lambda_{2PA}) = \frac{F_S(\lambda_{2PA})C_R f_R(\lambda_{1PA})}{F_R(\lambda_{2PA})C_S f_S(\lambda_{1PA})}\sigma_{2PA}^{R}(\lambda_{2PA})\frac{1-10^{-O.D.(\lambda_{1PA})S}}{1-10^{-O.D.(\lambda_{1PA})R}}$$

where F is measured 2PEF signal, C is concentration, f is 1PEF signal, S is the sample, R is the reference, and OD is the absorbance of the sample.

3. Experimental results

3.1 YP3

3.1.1 Molar absorption spectrum

The molar absorption of YP3 was calculated from a weighed mass of 0.0015 g (3.9 µM) of YP3 solid (M.W. = 381.44 g/mol) dissolved in 25 mL of MeOH, which was added dropwise in 25 µL increments to a solution of 3 mL MeOH. The increase in absorption from these additions is shown in Figure 11, with absorption maxima at 301 nm and 283 nm, accompanied by a minor peak at 292 nm and a shoulder around 270 nm. Additionally, absorption appears below 230 nm, although the focus of this thesis is on the lowest energy transition. Fitting the observed increases in absorption with Beers law for all wavelengths, exemplified on the right, resulted in a molar absorption of 77000 ± 2000 $M^{-1}cm^{-1}$ at 301 nm.

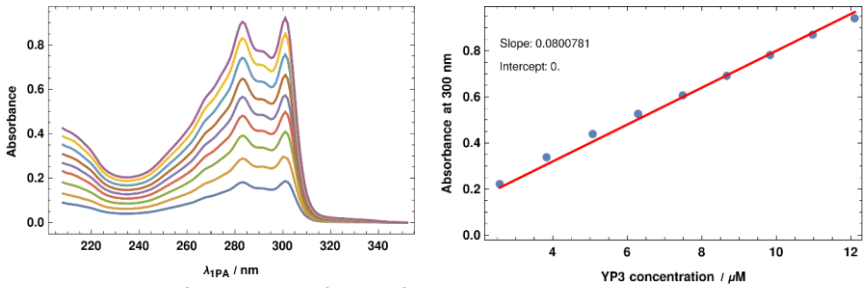

Figure 11. Calculation of molar absorption for YP3. Left displays increased absorbance observed with additions of concentrated YP3. Right displays an example linear fit at 300 nm.

The main absorption features, shown in Figure 12, closely resemble the spectrum of diphenylacetylene (DPA), which shows sharp bands at 297.5, 280.5 nm in methylcyclohexane, and has a molar absorption maximum of 23400 $M^{-1}cm^{-1}$,[41] roughly 1/3 that of YP3. However, YP3 additionally displays a very weak absorption band at longer wavelengths, which is absent in the DPA spectrum.

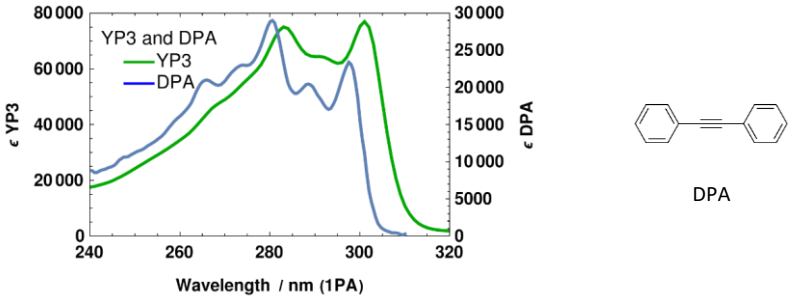

Figure 12. The molar absorption spectrum of YP3 in methanol, compared to a spectrum of diphenylacetylene in methylcyclohexane from reference (left). Molecular representation of DPA (right) from ref 41.

3.1.2 One-photon titration of YP3 with Triflic Acid

Figure 13 depicts the change in absorbance during the protonation of YP3 with TFL, corrected for volume changes during titration. Initially, the spectrum exhibits characteristic sharp spectral bands, with prominent peaks of the neutral form. Increasing the concentration of TFL, which lowered pH in a nearly linear manner, the absorbance within the range of 280 - 301 nm diminishes, leading to a reduction in the intensity of the main peaks. At the same time, a dramatic increase in absorption is observed in a broad band centred at 325 nm. Closer inspection of spectra reveals several isosbestic points, suggesting a multiple step-wise reaction process. The first four spectra display an isosbestic point at 304.5 nm ($3 < pH < 5$), although this transitions slightly to a second stable point at 302 nm ($1 < pH < 3$). Further acidified solutions develop an extended ~5 nm region of nearly constant absorption around 297 nm ($pH < 1$). Additionally, this last transformation increases the absorption at 283 nm, although the spectrum remains broad. The final spectra also reveal the broad 325 nm maximum is accompanied by a similar broad shoulder near 305 nm.

The appearance of distinct isosbestic points is important, and can be compared to a similar ethynyl-benzene compound studied by Asselberghs et al.[42] who observe a single isosbestic point, which they interpret as a single protonation step. However, different isosbestic locations cannot be described by a single step process, confirming a multistep-process.

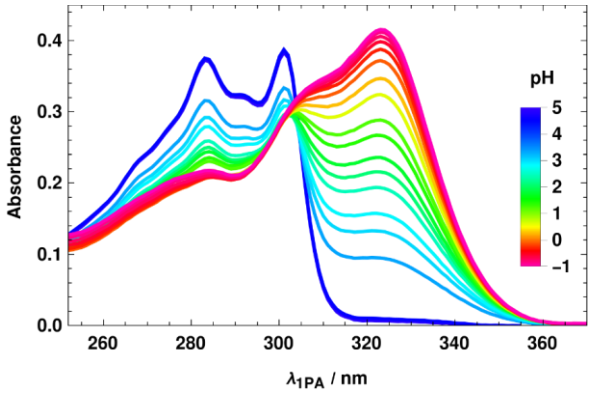

Figure 13. Titration of YP3 with triflic acid in methanol, corrected for the volume of added acid. The neutral solution is shown in blue, while strongly acidic solutions are in magenta.

Titration pH and spectral data was modelled using four equilibrium reactions, adhering to the three observed isosbestic points. Selection of this model was additionally supported by singular value decomposition of the absorption matrix, ***A***, which revealed the first four singular values comprise 95% of the total signal, with the remaining components appearing as a scree[43] indicative of random noise. Modelling employed three acid-base reaction equilibria, wherein YP3 protonated successively to H3YP3,

$$YP3 \xrightarrow{pK_1} HYP3 \xrightarrow{pK_2} H2YP3 \xrightarrow{pK_3} H3YP3$$

Producing three equilibrium equations with constants pK_1, pK_2, and pK_3, which paired with a sum of total concentration, C_{tot}, allowed for the solution of all four YP3 variable forms,

$$10^{-pK_1} = \frac{10^{-pH}[YP3]}{[HYP3]}$$

$$10^{-pK_2} = \frac{10^{-pH}[HYP3]}{[H2YP3]}$$

$$10^{-pK_3} = \frac{10^{-pH}[H2YP3]}{[H3YP3]}$$

$$C_{tot} = [YP3] + [HYP3] + [H2YP3] + [H3YP3]$$

Solving these four equations produced explicit models of concentration for all forms as a function of pH and estimates of pK_a,

$$[YP3] = \frac{10^{3pH} C_{tot}}{10^{3pH} + 10^{2pH+pK_1} + 10^{pH+pK_1+pK_2} + 10^{pK_1+pK_2+pK_3}}$$

$$[HYP3] = \frac{10^{2pH+pK_1} C_{tot}}{10^{3pH} + 10^{2pH+pK_1} + 10^{pH+pK_1+pK_2} + 10^{pK_1+pK_2+pK_3}}$$

$$[H2YP3] = \frac{10^{pH+pK_1+pK_2} C_{tot}}{10^{3pH} + 10^{2pH+pK_1} + 10^{H+pK_1+pK_2} + 10^{pK_1+pK_2+pK_3}}$$

$$[H3YP3] = \frac{10^{pK_1+pK_2+pK_3} C_{tot}}{10^{3pH} + 10^{2pH+pK_1} + 10^{H+pK_1+pK_2} + 10^{pK_1+pK_2+pK_3}}$$

With C_{tot} predetermined at 5.0 µM based on previous molar absorption measurement of YP3. This model was optimized using a multivariate curve resolution – alternating least squares (MCR-ALS) method[44] developed in house using Mathematica software.[6] Guesses of pK_a values ($pK_1 \rightarrow 3.2$, $pK_2 \rightarrow 2.8$, $pK_3 \rightarrow -0.8$) facilitated initial model construction. These produced concentrations associated with each spectrum according to the pH that was coincidentally measured, creating a list of concentrations for each reaction form combined as a matrix, $\boldsymbol{C}$. These concentrations were used to solve the associated molar absorption spectra, using the pseudoinverse, $\boldsymbol{C}^{+}$ in a matrix representation of Beers Law,

$$\boldsymbol{A} = \boldsymbol{\varepsilon}^{T} \cdot \boldsymbol{C} \cdot d$$

applying the pseudoinverse as,

$$\frac{\boldsymbol{A}}{d} \cdot \boldsymbol{C}^{+} \approx \boldsymbol{\varepsilon}^{T}$$

The resulting molar absorption spectra were in turn slightly corrected by making all values nonnegative, and their pseudo-inverse, $(\boldsymbol{\varepsilon}^{T})^{+}$, was again used to recalculate $\boldsymbol{C}$.

$$(\boldsymbol{\varepsilon}^{T})^{+} \cdot \frac{\boldsymbol{A}}{d} \approx \boldsymbol{C}$$

These new concentrations were fit with the reaction model, updating the pK_a's, and this procedure repeated until the pKa values converged to, $pK_1 = 3.35$, $pK_2 = 1.07$, $pK_3 = -1.25$. Notably the reaction steps occur with nearly equal gaps of ~2.3 pH units, displayed in Figure 14.

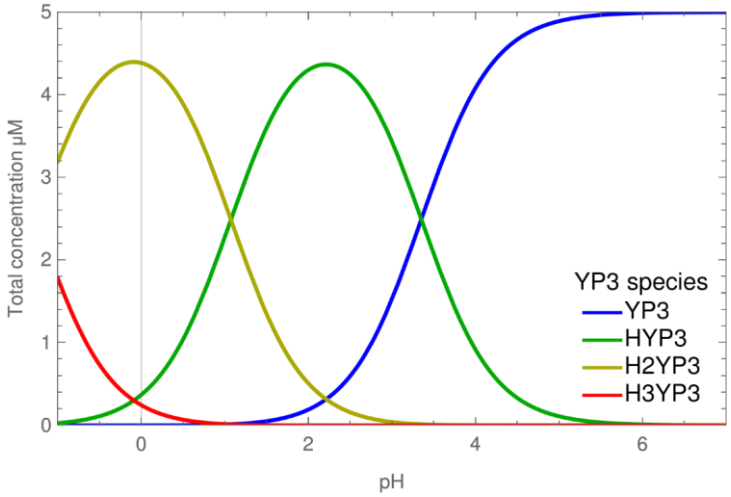

Figure 14. The pH-dependent concentration associated with the isolated spectra listed in Figure X. Notably, most acidic component was modelled to be only partially present, even for the lowest pH.

Commented [ZKH1]: I am confused here.

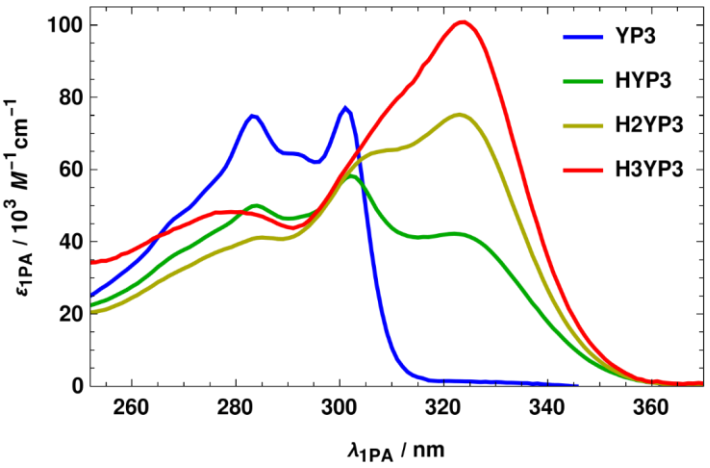

Figure 15. The optimized spectra for the four-component reaction model, representing acid-base forms YP3, HYP3, H2YP3, and H3YP3.

Figure 15 displays the four primary components identified from MCR-ALS optimization. These can be identified as the neutral form (YP3, blue line), a single protonation (HYP3, green line), double protonation (H2YP3, yellow line) and the fully protonated form (H3YP3, red line). Notably, all three protonated spectra display a similar low-energy feature, with maximum at 323, 324, and 325 nm for first, second and third protonation. This feature increases in intensity almost equally for each protonation step. One may also observe some recreation of the isosbestic points in the spectral profiles, where blue and green spectra overlap at 304.5 nm, while green, yellow and red all overlap near 300 nm. These spectra were used to calibrate the concentrations of samples used in 2PA, fitting the associated 1PA spectra to determine concentrations of YP3, HYP3, H2YP3 and H3YP3.

3.1.3 Fluorescence (emission)

Figure 16 depicts the emission spectra of all YP3 compounds. The neutral form YP3 (blue line) displays a bright emission with a maximum of 350 nm, while intermediate protonation forms HYP3 and H2YP3 (green line) have seemingly identical spectra that is substantially red-shifted to 470 nm. Finally, the fully-protonated form H3YP3 (red dotted line) appeared to have no emission in the 1PA measurement, although perhaps a minor signal was observed during 2PA excitation. While quantum yields were not measured, it is clear that YP3 is substantially more fluorescent than all other forms.

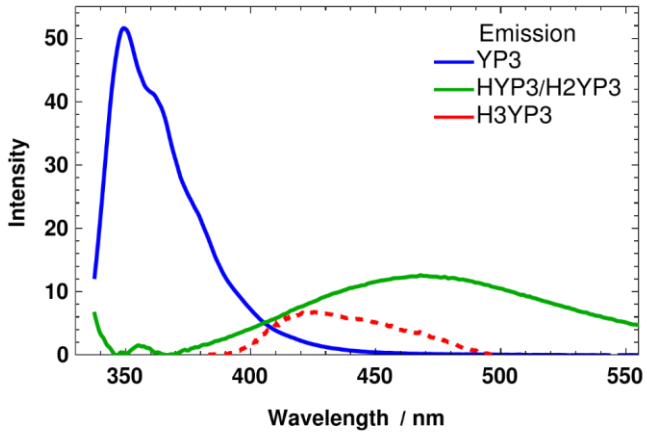

Figure 16. Fluorescence spectra of YP3, HYP3/H2YP3, H3YP3.

3.1.4 One- and Two-Photon Absorption

Two photon spectra were collected for all four YP3 forms, estimated from combining spectra of 7 samples with different concentrations of triflic acid, attempting to maximize the concentrations from Figure 14. These are shown in Figures 17-20 compared to 1PA model spectra from Figure 15, with the 2PA cross section aligned with the bottom-left axes and molar extinction corresponding to the top-right. Dark red points indicate measurements of absolute 2PA cross section.

After accounting for the difference in wavelength, all observed 2PA spectra appear similar to the associated 1PA maximum, albeit with the exception of a subtle red peak at 620 nm. However, in each case, there is also an extended 2PA red-edge which no longer matches with 1PA. In the case of the neutral form, this red-edge shift is only ~3 nm, but grows to ~11 nm for both partially-protonated forms. In the case of the fully protonated form, which did not appear to fluoresce, the two-photon excited fluorescence measurement was unable to observe much other than an obscure possible feature that does not appear to match the 1PA spectrum.

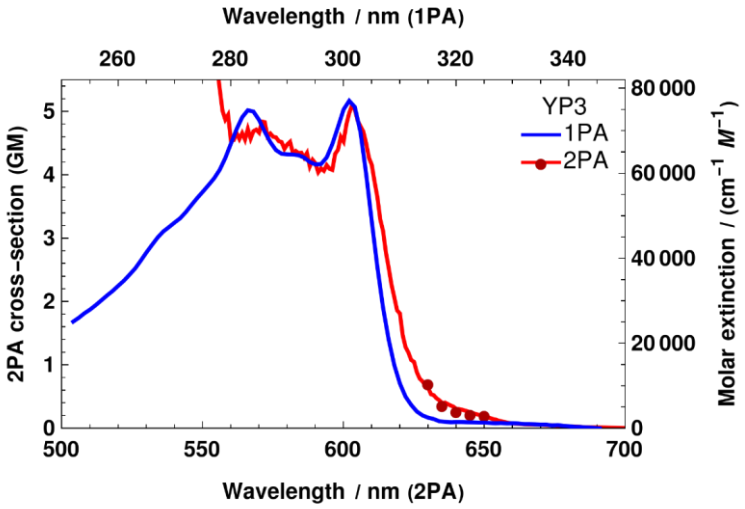

Figure 17.Optical absorption cross sections for YP3 in methanol. 1PA (Blue line, right axis) and 2PA (Red line, left axis), absolute absorption (dark red dots).

The cross section of the neutral form appears to maximize at ~5 GM, but notable enhancement in 2PA is seen for both HYP3 and H2YP3, which have respective cross section maxima of 22 GM and 14 GM at the main peak. This contrasts the changes in 1PA, where the first protonation form decreases in molar absorption to ~60000 $M^{-1}cm^{-1}$, while the YP3 and H2YP3 spectra have peaks close to ~80000 $M^{-1}cm^{-1}$.

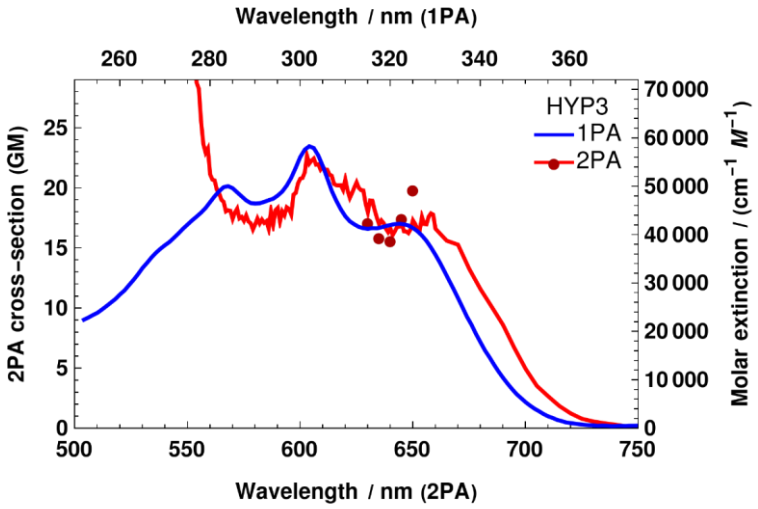

Figure 18. Optical absorption cross sections for HYP3 in methanol. 1PA (Blue line, right axis) and 2PA (Red line, left axis), absolute absorption (dark red dots).

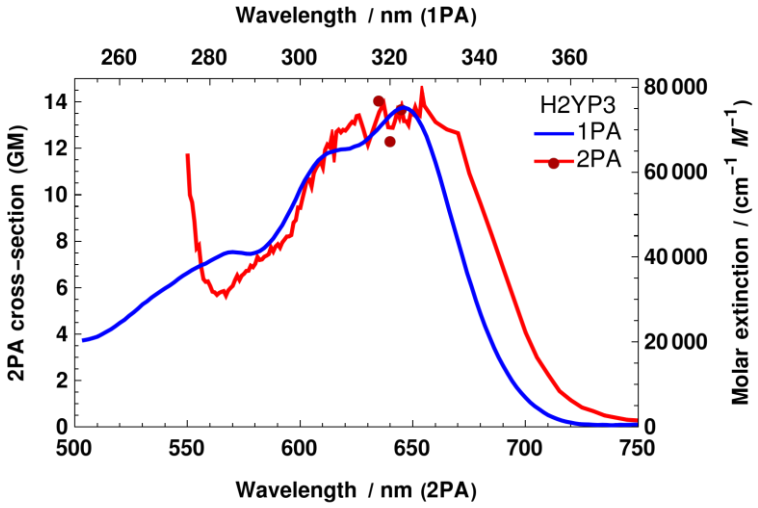

Figure 19. Optical absorption cross sections for H_2YP3 in methanol. 1PA (Blue line, right axis) and 2PA (Red line, left axis), absolute absorption (dark red dots).

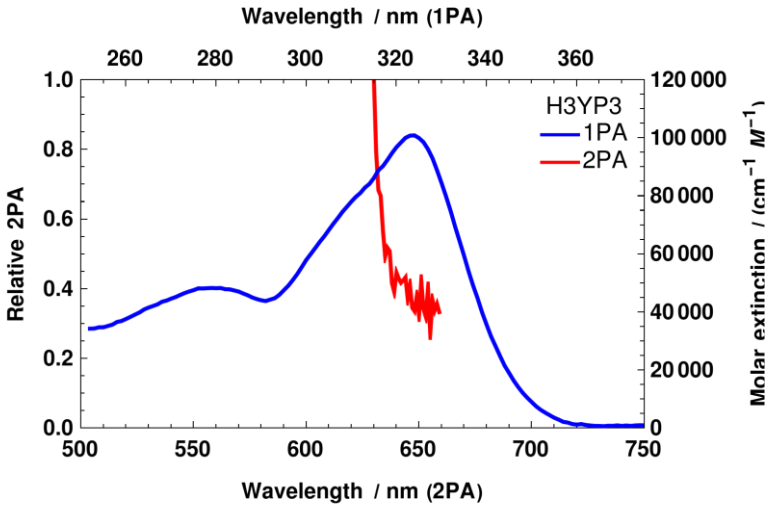

Figure 20. Optical absorption cross sections for H3P3 in methanol. 1PA (Blue line, right axis) and 2PA (Red line, left axis), absolute absorption (dark red dots).

3.2 2AP

3.2.1 Titration with H_2SO_4 and spectral changes

Due to the 2-amino group on 2AP, protonation can occur on the periphery of the conjugated centre, enabling two molecular forms:

$$2AP \rightarrow H2AP^{+}$$

The neutral form of the compound exhibits its highest peak at 305 nm, with volume-corrected absorbance of 0.49 (Figure 21). Upon addition of acid, this peak shifts towards longer wavelengths, accompanied by a decrease in absorbance, finally stabilizing with a maximum wavelength at 315 nm and absorbance of 0.32. Notably, there are two distinct isosbestic points observed at 266 and 321 nm. Despite these shifts, the spectra of the neutral and protonated forms of 2AP maintain a similar same shape, similar excitation behaviour, and preservation chromophore's conjugated structure. The initial and final reading were selected to represent the neutral 2AP and its protonated form, H2AP respectively.

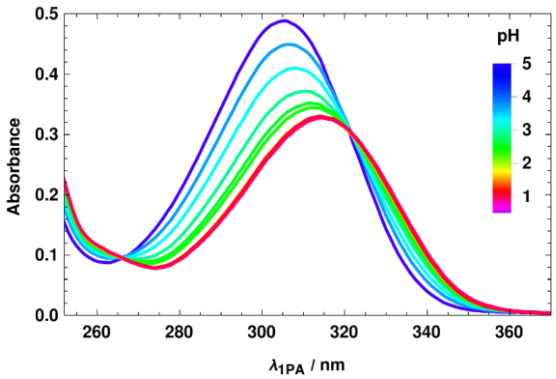

Figure 21. The volume-corrected absorption of 2AP in H_2O titrated with H_2SO_4, with colour denoting the measured pH for each spectrum.

The figure 22, presents the molar absorption spectra for neutral and protonated forms of 2AP. The maximum absorption of 2AP is at 305 nm with 5560 $M^{-1}cm^{-1}$, and displays a second absorption band below 260 nm. The H2AP form has its peak at 314 nm with a molar absorbance of 3703 $M^{-1}cm^{-1}$, and the feature below 260 nm is also revealed to have an extended tail to 275 nm The two spectra overlap at isosbestic points located near 241, 266 and 321 nm.

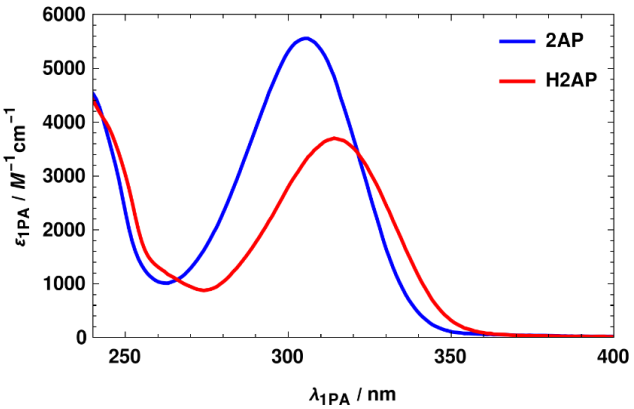

Figure 22. The molar absorption spectra for 2AP and H2AP in distilled water and 0.1 M sulfuric acid, respectively.

3.2.2. Two-photon absorption and polarisation ratio of 2AP and H2AP

Figure 23 compares the one- and two-photon cross sections of 2AP, along with the two-photon polarization ratio. Notably, the 2PA spectral shape deviates slightly from the 1PA, appearing to shift slightly to the red, with a maximum wavelength at 620 nm having cross section of 0.12 GM. While this cross section was scaled to match a previous 2PA measurement of the same system, they

observe a more close spectral match to the 1PA band.[45] The measured polarization ratio, shown as an inset, displays a gradual variation over the width of the absorption band, changing from Ω = 1.18 at 700 nm to Ω = 1.02 at 600 nm.

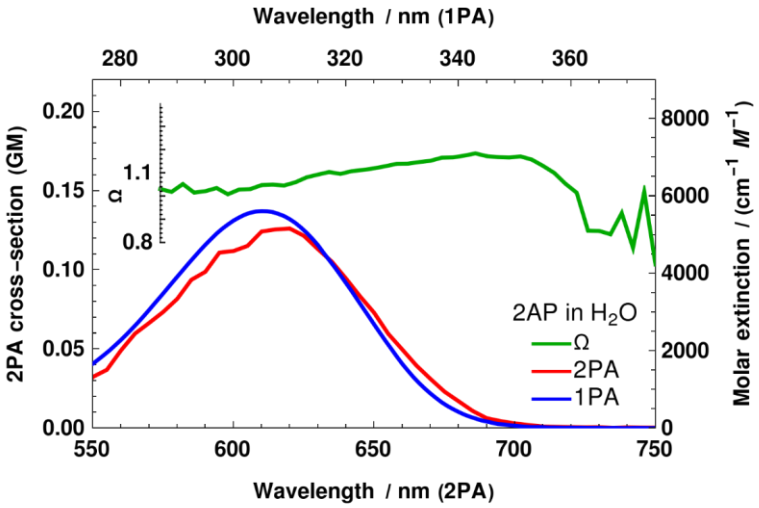

Figure 23. Comparison of one- and two-photon cross sections for 2AP in H_2O. The 2PA spectrum (red, left/bottom axes) is slightly shifted compared to the 1PA spectrum (blue, right/top axes). Also displayed is the 2PA polarization ratio (green, bottom and inset axis).

A similar comparison for H2PA in H_2SO_4 is shown in Figure 24. Here, the shift in 2PA compared to 1PA is even more dramatic, with a maximum 2PA cross section of 0.3 at 645 nm. The discrepancy between 1PA and 2PA peak wavelengths is in this case (λ_{2PA} - $2\lambda_{1PA}$ ~ 17 nm) is nearly twice that of the neutral form (λ_{2PA} - $2\lambda_{1PA}$ ~ 10 nm). The cross-section value of this peak, measured explicitly in this case, displays an enhancement of 2PA compared to the neutral form, although the two points do also show significant variation. The polarization ratio is also notably noisier than in the neutral case, likely reflecting a lower 2PEF signal from the sample. However, a similar gradual trend may still be seen over the spectral band, with points near 700 nm close to Ω = 1.1, while the 600 nm region is closer to Ω = 1.0.

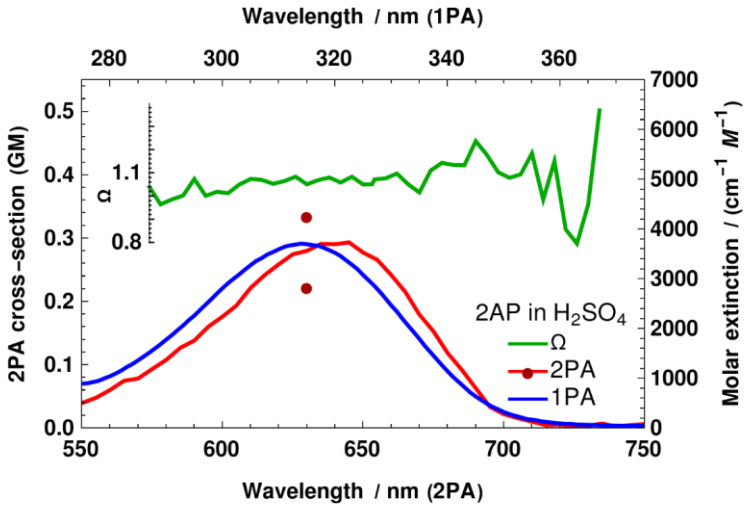

Figure 24. One- and two-photon absorption cross section spectra for H2AP in 0.1 M H_2SO_4. In addition to 2PA spectral shapes analogous to the neutral sample, the absolute cross section was also determined at 630 nm, shown as dark-red dots.

4. Discussion

4.1 YP3

1. neutral form

The main 1PA absorbance band at 301 nm of YP3 closely resembles the DPA spectrum, albeit shifted by 5 nm to the red.[41] This resemblance could be interpreted as the absence of conjugation through the YP3 centre. However, the weak shoulder extending to 340 nm, indicates a lower energy state that is impossible for the DPA monomer. Importantly, fluorescence from YP3 has a maximum of 350 nm, originating from this forbidden state. Furthermore, in 2PA, a similar shoulder appears at 680 nm with an additional feature at 650 nm, possibly indicating vibronic coupling. However, more computational analysis is needed to describe such coupling effects.

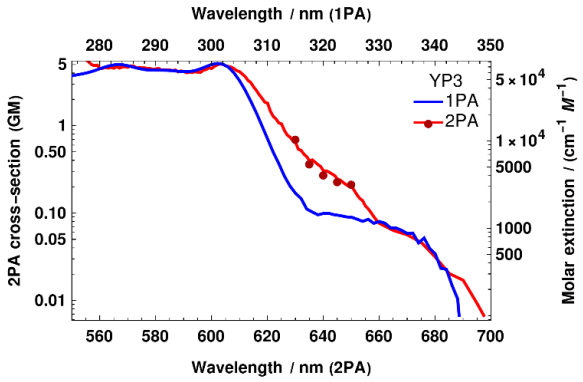

Figure 25. Logarithmic scale of YP3 1PA and 2PA spectra. The low-energy shoulder in 1PA is partially reproduced in 2PA, but 2PA displays an additional absorption feature.

This indication of conjugation throughout of YP3 suggests D_{3h} molecular symmetry. The agreement between 1PA and 2PA around 301 nm therefore, must be an E' symmetric transition as this is the only symmetry allowed for both processes;[46] transforming as (x,y) in 1PA, and ($x^2 - y^2$, xy) in 2PA according to their respective symmetry rules.

The protonated form.

Upon protonation, both HYP3 and H2YP3 presumably break the D_{3h} molecular symmetry, so should behave more like a push-pull dipolar system.[13,47] Consequently, we observe an increase in the total observed 2PA cross section, and fairly good agreement between 1PA and 2PA in the main absorption region. On the red edge for both intermediate forms there is a red shift of absorbance, λ_{2PA} = 11 nm. This is unlikely to be a forbidden transition as the symmetry should be broken. However, emission spectra for both forms is identical and matches with DPA phosphorescence, suggesting emission may come from one branch and have competing relaxation pathways. Alternatively, there might be several ground state rotamer or other electronic configurations which appear differently for 2PA. However, more analysis is required to understand this red shift.

Another explanation for this red shift is that conjugation throughout the molecule is completely broken and excitation only occurs on single branches. Recent measurements by Ishii et. al.[13] demonstrate significant red shifts in DPA absorbance upon addition of strong electron withdrawing groups (-NO_2) at one end, closely matching our protonated observations. In particular, DPA-NO_2 shows a 1PA peak at 325 nm and in 2PA, a sharp rise below 550 nm and a gradual increase in cross section above 570 nm. Thus, we cannot rule out the possibility that upon symmetry breaking the YP3 chromophore is split into separate branches. However, we do not see the evidence of dual emission, so excitation relaxes to a single emitter.

Unfortunately, the fully-protonated compound did not produce enough fluorescence to observe its spectral features or absolute cross-section. The results we display are difficult to interpret and may be influenced by noise due to these low signals. This may indicate that protonated branches quench fluorescence. In the case of intermediate forms, if excitations are localised on a single branch, such quenching would imply inter-branch hopping does not occur. The concept of isolated excitations matches kinetic descriptions of a similar octopolar-triazine system reported by Vauthey et. al.[12] whereby the alkyne bridge photoisomerizes to an allene stabilising charge separation in the excited state.
Taking together the quenching that occurs on protonated branches would not be observed in intermediate forms. In this case, emission must come from the neutral branches where localisation drives a similar isomerisation, further relaxing to the emissive triplet state.[48] This isomerisation process does not occur to significant amount in neutral form, which could be a further indication of delocalisation. It is possible that not enough electron density shifts to any one branch to initiate the isomerisation leading to the triplet.

4.2 2AP

The discrepancy between 1PA and 2PA spectra for both neutral 2AP and protonated H2PA samples may be understood according to the tautomerization of the 7H- and 9H- forms. A study by Neely et al.[34] uncovered that this tautomerization produces differences in the excited state lifetimes, and slightly shifts the maximum emission of the 9H- tautomer ~7 nm shorter compared to the 7H-tautomer. This study additionally suggested that the absorption profiles of the two forms was also shifted, with 9H transitions again at shorter wavelengths. Thus, we may attempt to separate the gradual changes observed in polarization ratio, as well as discrepancies between 1PA and 2PA spectral profiles, to relative amounts of 7H- and 9H- absorption. In a simple model, we may assume that both absorption spectra of each tautomer correspond to a two-level description, wherein 1PA and 2PA spectral profiles are identical, but may be scaled differently as a result of permanent dipole effects in 2PA. The polarization ratio for each form is also constant over all wavelengths, signifying that the angle of permanent and transition dipoles is wavelength independent, although this angle differs between the two tautomers. The values of these two polarization ratios are selected as the maximum and minimum observed values in the main absorption band, shown as dashed lines in Figure 26.

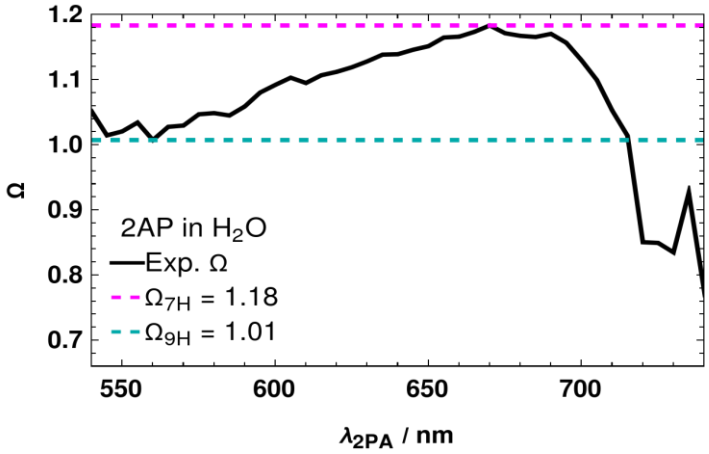

Figure 26. Polarization ratio and estimated ratios for the tautomers according to maximum/minimum observations.

Using these two extremes, Ω_{7H} and Ω_{9H}, we may estimate the contribution of 2PA signal arising from each tautomer according to the relative value of the observed polarization ratio,

$$\rho_{7H} = \frac{(\Omega - \Omega_{9H})}{(\Omega_{7H} - \Omega_{9H})}$$

where ρ_{7H} is the relative proportion of 7H signal in the 2PA measurement. Similarly, the proportion of 9H would be classified, $\rho_{9H} = 1 - \rho_{7H}$. This analysis is based on a similar method which successfully separated transitions of different symmetry in a single molecular system.[49] The separated 2PA spectra, shown in Figure 27, reveal two absorption bands of similar intensity and shape. These same profiles may be scaled to match the 1PA spectrum, notably requiring a relative increase of 1.4 9H : 7H signal is required to optimally match 1PA spectra. According to the two-level model, this indicates that the permanent dipole moment of the 9H tautomer is reduced compared to 7H. The ratio of the 9H and 7H signal replicating the 1PA spectrum also coincides with the ratios of ~ 60% 9H : 40% 7H estimated by Neely et al.[34]

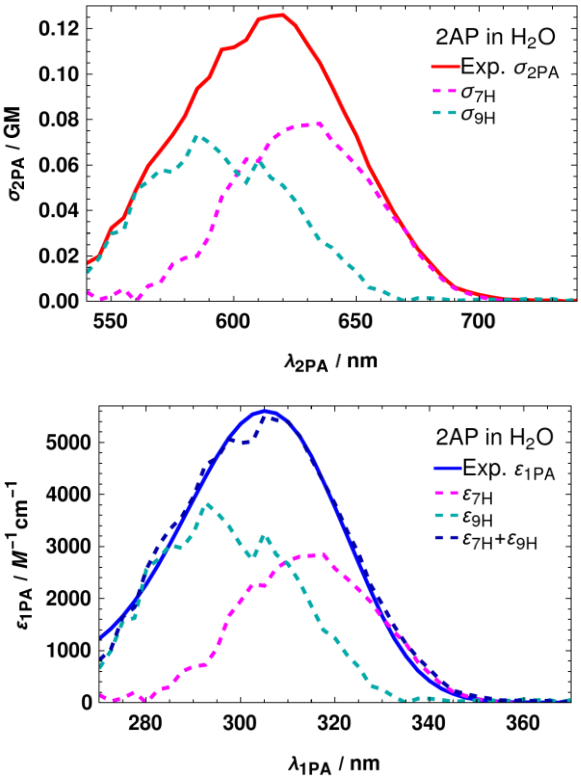

Figure 27. Top: Separation of 2PA spectrum according to polarization ratio model, showing that 7H 2PA signal is stronger than 9H. Bottom: Scaling the 2PA model spectra to best fit the 1PA spectrum, for which 9H becomes the larger feature.

Notably, the modelled shift in maximum absorption wavelength is ~ 25 nm, similar to estimated tautomeric shifts of ~22 nm in a thienoguanosine analogue.[33] This lends some support to the analysis method, although spectral descriptions would be better addressed if paired with better calculations of dipole angles and a more rigorous analysis.

Conclusions

In this thesis, 2PA spectral cross section was measured by fluorescence excitation using femtosecond pulses, paired with 1PA acid-based titrations, to understand interconversion in multi-ground state proton accepting chromophores, YP3 and 2AP. For both systems, we were able to separate several major ground state configurations and their associated spectral properties.

In the case of YP3 we used three stepwise protonation reactions as a tool to break an initially centrosymmetric chromophore into two strongly polar symmetry-broken forms, finally restoring the symmetry in the fully protonated form. Initial symmetry breaking red shifted absorption and quenched fluorescence, although phosphorescence was retained, apparently from excitations localised on a single branch of a molecule. However, further protonation produced much less change in photophysics, likely as a result of the same localisation processes, while complete quenching of fluorescence and phosphorescence occurred in the fully protonated case. The large changes in emission behaviour as well as charge transfer make this system interesting for both molecular sensing and photoredox chemistry.

For the DNA base analogue 2AP, protonation red shifted absorption, while maintaining a similar spectral shape. Both protonated and neutral forms demonstrated a notable discrepancy between 1PA and 2PA spectral shapes. At the same time, both forms also displayed a gradual change of 2PA polarisation ratio which could be modelled as an effect of tautomerisation between 9H and 7H isomers, revealing their individual spectra. This marks a significant experimental development in understanding the ground state nature of these interconverting forms and reveals an absorption shift of 25 nm.

These findings reveal the importance of nonlinear optics as sensitive methods for understanding complex ground state behaviour for symmetry agile systems that present multiple stable states. Particularly, they demonstrate how the comparison of 2PA and 1PA can uncover details that are missed by either measurement alone. Such multifaceted methods are valuable for the development of future multifunctional materials.

Acknowledgments

I am deeply grateful to my thesis supervisor, Charlie, for his outstanding mentorship and support throughout my research. His guidance, patience and expertise have been invaluable, and I appreciate his dedication to my academic growth.
Thank you for an enriching and rewarding experience.

References

(1) Green, J. E.; Wook Choi, J.; Boukai, A.; Bunimovich, Y.; Johnston-Halperin, E.; DeIonno, E.; Luo, Y.; Sheriff, B. A.; Xu, K.; Shik Shin, Y.; Tseng, H.-R.; Stoddart, J. F.; Heath, J. R. A 160-Kilobit Molecular Electronic Memory Patterned at 1011 Bits per Square Centimetre. *Nature* **2007**, *445* (7126), 414–417. https://doi.org/10.1038/nature05462.

(2) Kawata, S.; Kawata, Y. Three-Dimensional Optical Data Storage Using Photochromic Materials. *Chem. Rev.* **2000**, *100* (5), 1777–1788. https://doi.org/10.1021/cr980073p.

(3) Champagne, B.; Plaquet, A.; Pozzo, J.-L.; Rodriguez, V.; Castet, F. Nonlinear Optical Molecular Switches as Selective Cation Sensors. *J. Am. Chem. Soc.* **2012**, *134* (19), 8101–8103. https://doi.org/10.1021/ja302395f.

(4) Lewandowski, B.; De Bo, G.; Ward, J. W.; Papmeyer, M.; Kuschel, S.; Aldegunde, M. J.; Gramlich, P. M. E.; Heckmann, D.; Goldup, S. M.; D'Souza, D. M.; Fernandes, A. E.; Leigh, D. A. Sequence-Specific Peptide Synthesis by an Artificial Small-Molecule Machine. *Science* **2013**, *339* (6116), 189–193. https://doi.org/10.1126/science.1229753.

(5) Schweighauser, L.; Häussinger, D.; Neuburger, M.; Wegner, H. A. Symmetry as a New Element to Control Molecular Switches. *Org. Biomol. Chem.* **2014**, *12* (21), 3371. https://doi.org/10.1039/c4ob00230j.

(6) Stark, C. W.; Rammo, M.; Trummal, A.; Uudsemaa, M.; Pahapill, J.; Sildoja, M.-M.; Tshepelevitsh, S.; Leito, I.; Young, D. C.; Szymański, B.; Vakuliuk, O.; Gryko, D. T.; Rebane, A. On-off-on Control of Molecular Inversion Symmetry via Multi-stage Protonation: Elucidating Vibronic Laporte Rule. *Angew. Chem. Int. Ed.* **2022**, e202212581. https://doi.org/10.1002/anie.202212581.

(7) Zewail, A. H. Femtochemistry: Atomic-Scale Dynamics of the Chemical Bond. *J. Phys. Chem. A* **2000**, *104* (24), 5660–5694. https://doi.org/10.1021/jp001460h.

(8) Suhling, K.; French, P. M. W.; Phillips, D. Time-Resolved Fluorescence Microscopy. *Photochem. Photobiol. Sci.* **2005**, *4* (1), 13–22. https://doi.org/10.1039/b412924p.

(9) Kukura, P.; McCamant, D. W.; Mathies, R. A. Femtosecond Stimulated Raman Spectroscopy. *Annu. Rev. Phys. Chem.* **2007**, *58* (1), 461–488. https://doi.org/10.1146/annurev.physchem.58.032806.104456.

(10) Maiuri, M.; Garavelli, M.; Cerullo, G. Ultrafast Spectroscopy: State of the Art and Open Challenges. *J. Am. Chem. Soc.* **2020**, *142* (1), 3–15. https://doi.org/10.1021/jacs.9b10533.

(11) Kraus, P. M.; Zürch, M.; Cushing, S. K.; Neumark, D. M.; Leone, S. R. The Ultrafast X-Ray Spectroscopic Revolution in Chemical Dynamics. *Nat. Rev. Chem.* **2018**, *2* (6), 82–94. https://doi.org/10.1038/s41570-018-0008-8.

(12) Vauthey, E. Photoinduced Symmetry-Breaking Charge Separation. *ChemPhysChem* **2012**, *13* (8), 2001–2011. https://doi.org/10.1002/cphc.201200106.

(13) Ishii, T.; Isozaki, T.; Kinoshita, S.; Takeuchi, R.; Kashihara, W.; Suzuki, T. A Substituent Effect on Two-Photon Absorption of Diphenylacetylene Derivatives with an Electron-Donating/Withdrawing Group. *J. Phys. Chem. A* **2021**, *125* (8), 1688–1695. https://doi.org/10.1021/acs.jpca.0c10545.

(14) Morales-Saavedra, O. G.; Ontiveros-Barrera, F. G.; Hennrich, G.; Mata-Zamora, M. E.; Rodríguez-Rosales, A. A.; Bañuelos, J. G. Spectroscopic and Nonlinear Photophysical Characterization of Organic Octupolar-Compounds Supported by Anodic-Alumina Nanotube-Arrays. *Mater. Sci. Eng. B* **2011**, *176* (18), 1479–1496. https://doi.org/10.1016/j.mseb.2011.09.018.

(15) McClain, W. M. Two-Photon Molecular Spectroscopy. *Acc. Chem. Res.* **1974**, *7* (5), 129–135. https://doi.org/10.1021/ar50077a001.

(16) Callis, P. R. The Theory of Two-Photon-Induced Fluorescence Anisotropy. In *Topics in Fluorescence Spectroscopy: Volume 5: Nonlinear and Two-Photon-Induced Fluorescence*;

Lakowicz, J. R., Ed.; Topics in Fluorescence Spectroscopy; Springer US: Boston, MA, 2002; Vol. 5, pp 1–42. https://doi.org/10.1007/0-306-47070-5_1.
(17) Boyd, R. W. Optically Induced Damage and Multiphoton Absorption. In *Nonlinear Optics*; Academic Press: Rochester, NY, 2008; pp 543–560.
(18) Swinehart, D. F. The Beer-Lambert Law. *J. Chem. Educ.* **1962**, *39* (7), 333–335.
(19) Göppert-Mayer, M. Elementary Processes with Two Quantum Transitions. *Ann. Phys.* **2009**, *18* (7–8), 466–479. https://doi.org/10.1002/andp.200910358.
(20) Paul, P. M.; Toma, E. S.; Breger, P.; Mullot, G.; Augé, F.; Balcou, Ph.; Muller, H. G.; Agostini, P. Observation of a Train of Attosecond Pulses from High Harmonic Generation. *Science* **2001**, *292* (5522), 1689–1692. https://doi.org/10.1126/science.1059413.
(21) McClain, W. M. Excited State Symmetry Assignment through Polarized Two-photon Absorption Studies of Fluids. *J. Chem. Phys.* **1971**, *55* (6), 2789–2796. https://doi.org/10.1063/1.1676494.
(22) Rebane, A.; Wicks, G.; Drobizhev, M.; Cooper, T.; Trummal, A.; Uudsemaa, M. Two-Photon Voltmeter for Measuring a Molecular Electric Field. *Angew. Chem. Int. Ed.* **2015**, *54* (26), 7582–7586. https://doi.org/10.1002/anie.201502157.
(23) Strickler, S. J.; Berg, R. A. Relationship between Absorption Intensity and Fluorescence Lifetime of Molecules. *J. Chem. Phys.* **1962**, *37* (4), 814–822. https://doi.org/10.1063/1.1733166.
(24) Swathi, K.; Sujith, M.; Divya, P. S.; P, M. V.; Delledonne, A.; Phan Huu, D. K. A.; Di Maiolo, F.; Terenziani, F.; Lapini, A.; Painelli, A.; Sissa, C.; Thomas, K. G. From Symmetry Breaking to Symmetry Swapping: Is Kasha's Rule Violated in Multibranched Phenyleneethynylenes? *Chem. Sci.* **2023**, *14* (8), 1986–1996. https://doi.org/10.1039/D2SC05206G.
(25) Mertz, E. L.; Tikhomirov, V. A.; Krishtalik, L. I. Stokes Shift as a Tool for Probing the Solvent Reorganization Energy. *J. Phys. Chem. A* **1997**, *101* (19), 3433–3442. https://doi.org/10.1021/jp963042b.
(26) Liu, J.; Lam, J. W. Y.; Tang, B. Z. Acetylenic Polymers: Syntheses, Structures, and Functions. *Chem. Rev.* **2009**, *109* (11), 5799–5867. https://doi.org/10.1021/cr900149d.
(27) Kivala, M.; Diederich, F. Acetylene-Derived Strong Organic Acceptors for Planar and Nonplanar Push−Pull Chromophores. *Acc. Chem. Res.* **2009**, *42* (2), 235–248. https://doi.org/10.1021/ar8001238.
(28) Oliva, M. M.; Casado, J.; López Navarrete, J. T.; Hennrich, G.; van Cleuvenbergen, S.; Asselberghs, I.; Clays, K.; Ruiz Delgado, M. C.; Brédas, J.; Seixas de Melo, J. S.; De Cola, L. Synthesis, Spectroscopy, Nonlinear Optics, and Theoretical Investigations of Thienylethynyl Octopoles with a Tunable Core. *Chem. Eur. J.* **2009**, *15* (33), 8223–8234. https://doi.org/10.1002/chem.200900702.
(29) Mikhaylov, A.; Uudsemaa, M.; Trummal, A.; Arias, E.; Moggio, I.; Ziolo, R.; Cooper, T. M.; Rebane, A. Spontaneous Symmetry Breaking Facilitates Metal-to-Ligand Charge Transfer: A Quantitative Two-Photon Absorption Study of Ferrocene-Phenyleneethynylene Oligomers. *J. Phys. Chem. Lett.* **2018**, *9* (8), 1893–1899. https://doi.org/10.1021/acs.jpclett.8b00525.
(30) LeCours, S. M.; Guan, H.-W.; DiMagno, S. G.; Wang, C. H.; Therien, M. J. Push-Pull Arylethynyl Porphyrins: New Chromophores That Exhibit Large Molecular First-Order Hyperpolarizabilities. *J. Am. Chem. Soc.* **1996**, *118* (6), 1497–1503.
(31) Marian, C. M. The Guanine Tautomer Puzzle: Quantum Chemical Investigation of Ground and Excited States. *J. Phys. Chem. A* **2007**, *111* (8), 1545–1553. https://doi.org/10.1021/jp068620v.
(32) Thoburn, J. D.; Lüttke, W.; Benedict, C.; Limbach, H.-H. Indigodiimine: A Highly Fluxional Molecule That Tautomerizes via Double Proton Transfers. *J. Am. Chem. Soc.* **1996**, *118* (49), 12459–12460. https://doi.org/10.1021/ja962515p.
(33) Sholokh, M.; Improta, R.; Mori, M.; Sharma, R.; Kenfack, C.; Shin, D.; Voltz, K.; Stote, R. H.; Zaporozhets, O. A.; Botta, M.; Tor, Y.; MØly, Y. Tautomers of a Fluorescent G Surrogate and

Their Distinct Photophysics Provide Additional Information Channels. *Angew. Chem. Int. Ed.* **2016**.
(34) Neely, R. K.; Magennis, S. W.; Dryden, D. T. F.; Jones, A. C. Evidence of Tautomerism in 2-Aminopurine from Fluorescence Lifetime Measurements. *J. Phys. Chem. B* **2004**, *108* (45), 17606–17610. https://doi.org/10.1021/jp0490857.
(35) He, R.-X.; Duan, X.-H.; Li, X.-Y. Theoretical Investigation of Spectral Properties and Tautomerization Mechanism of 2-Aminopurine. *Phys. Chem. Chem. Phys.* **2006**, *8* (5), 587–591. https://doi.org/10.1039/B512242B.
(36) Rammo, M.; Trummal, A.; Uudsemaa, M.; Pahapill, J.; Petritsenko, K.; Sildoja, M.; Stark, C. W.; Selberg, S.; Leito, I.; Palmi, K.; Adamson, J.; Rebane, A. Novel Lipophilic Fluorophores with Highly Acidity-Dependent Two-Photon Response. *Chem. Eur. J.* **2022**, *28* (8), e202103707. https://doi.org/10.1002/chem.202103707.
(37) Morales, D. A. Mathematical Modeling of Titration Curves. *J. Chemom.* **2002**, *16* (5), 247–260. https://doi.org/10.1002/cem.719.
(38) de Reguardati, S.; Pahapill, J.; Mikhailov, A.; Stepanenko, Y.; Rebane, A. High-Accuracy Reference Standards for Two-Photon Absorption in the 680–1050 Nm Wavelength Range. *Opt. Express* **2016**, *24* (8), 9053–9066. https://doi.org/10.1364/OE.24.009053.
(39) Rebane, A. *2PADB*. Two-photon absorption (2PA) spectra database. https://kbfi.ee/mpa/.
(40) Makarov, N. S.; Drobizhev, M.; Rebane, A. Two-Photon Absorption Standards in the 550–1600 Nm Excitation Wavelength Range. *Opt. Express* **2008**, *16* (6), 4029–4047. https://doi.org/10.1364/OE.16.004029.
(41) Saltiel, J.; Kumar, V. K. R. Photophysics of Diphenylacetylene: Light from the "Dark State." *J. Phys. Chem. A* **2012**, *116* (43), 10548–10558. https://doi.org/10.1021/jp307896c.
(42) Asselberghs, I.; Hennrich, G.; Clays, K. Proton-Triggered Octopolar NLO Chromophores. *J. Phys. Chem. A* **2006**, *110* (19), 6271–6275. https://doi.org/10.1021/jp061452m.
(43) Cattell, R. B. The Scree Test For The Number Of Factors. *Multivar. Behav. Res.* **1966**, *1* (2), 245–276. https://doi.org/10.1207/s15327906mbr0102_10.
(44) de Juan, A.; Jaumot, J.; Tauler, R. Multivariate Curve Resolution (MCR). Solving the Mixture Analysis Problem. *Anal. Methods* **2014**, *6* (14), 4964–4976. https://doi.org/10.1039/C4AY00571F.
(45) Mikhaylov, A.; de Reguardati, S.; Pahapill, J.; Callis, P. R.; Kohler, B.; Rebane, A. Two-Photon Absorption Spectra of Fluorescent Isomorphic DNA Base Analogs. *Biomed. Opt. Express* **2018**, *9* (2), 447. https://doi.org/10.1364/BOE.9.000447.
(46) Vincent, A. *Molecular Symmetry and Group Theory : A Programmed Introduction to Chemical Applications*, 2nd ed.; Wiley, 2001.
(47) List, N. H.; Zaleśny, R.; Murugan, N. A.; Kongsted, J.; Bartkowiak, W.; Ågren, H. Relation between Nonlinear Optical Properties of Push–Pull Molecules and Metric of Charge Transfer Excitations. *J. Chem. Theory Comput.* **2015**, *11* (9), 4182–4188. https://doi.org/10.1021/acs.jctc.5b00538.
(48) Krämer, M.; Bunz, U. H. F.; Dreuw, A. Comprehensive Look at the Photochemistry of Tolane. *J. Phys. Chem. A* **2017**, *121* (5), 946–953. https://doi.org/10.1021/acs.jpca.6b09596.
(49) Callis, P. R.; Scott, T. W.; Albrecht, A. C. Polarized Two-photon Fluorescence Excitation Studies of Pyrimidine. *J. Chem. Phys.* **1981**, *75* (12), 5640–5646. https://doi.org/10.1063/1.442003.